Infrared spectrum of the ν_2 vibration-inversion band of H_3O^+

Di-Jia Liu, Nathan N. Haese,[a] and Takeshi Oka
Departments of Chemistry and Astronomy and Astrophysics, The University of Chicago, Chicago, Illinois 60637

(Received 30 November 1984; accepted 13 March 1985)

High resolution infrared spectra of the $1^- \leftarrow 0^+$ and $1^+ \leftarrow 0^-$ ν_2 vibration-inversion bands of H_3O^+ have been observed in the ac glow discharge by using tunable diode lasers and the velocity modulation technique. The two band origins were found to be at 954.4003(25) and 525.8237(13) cm^{-1} for the $1^- \leftarrow 0^+$ and $1^+ \leftarrow 0^-$ bands, respectively. The band origins, rotational constants, and observed relative band strengths are compared with predictions based on *ab initio* theory. The discharge chemistry of H_3O^+ is discussed with reference to the observed line strength-gas composition relation and known ion–molecule reactions.

I. INTRODUCTION

The oxonium molecular ion H_3O^+ is one of the most interesting molecular ions because of its special position as the mediator in aqueous solution chemistry,[1] its important role of transfering protons in biological systems,[2] and its anticipated abundance in dense interstellar clouds.[3–5] While infrared, Raman, and NMR spectra of H_3O^+ in solution and in crystal have been observed for over 30 years,[6–14] its gas phase spectrum was unknown until 1977 when Schwarz detected at low resolution the ν_3 stretching vibration by pulsed radiolysis.[15] The high resolution spectrum of the ν_3 band was first observed by Begemann, Gudeman, Pfaff, and Saykally using a color center laser and the ac discharge velocity modulation technique.[16]

The H_3O^+ ion is isoelectronic with NH_3 and it has a pyramidal structure with C_{3v} symmetry. The tunneling of oxygen atom through the plane of the hydrogen atoms results in the splitting of the energy levels of the ν_2 bending vibration as in the case of NH_3.[17] Figure 1 shows the vibration-inversion energy levels of the ground and first excited states of the ν_2 vibration and the associated potential energy. From the analysis of the vibration-rotation spectrum the vibration-inversion potential and molecular structure can be determined.[18–23] The observed infrared spectrum will make it possible to search for the spectrum of the H_3O^+ ion in interstellar space using an infrared telescope. When the vibration-inversion levels shown in Fig. 1 are completely analyzed and the ground state splitting between 0^+ and 0^- determined, it will also be possible to look for the interstellar H_3O^+ ion in the microwave and in the far infrared region.

There have been extensive theoretical studies of the inversion potential and rotation-inversion energy level of the ν_2 mode.[22,24–28] The experimental observation of the $1^- \text{–} 0^+$ band was first carried out by Haese and Oka[29] using a 10 μm diode laser and an ac glow discharge with the velocity modulation technique. Recently, Lemoine and Destombes[30] have reported the observation of several high J R-branch lines of the same band using a magnetically confined glow discharge. We report in this paper our observation of the $1^+ \text{–} 0^-$ band of the ν_2 vibration-inversion spectrum as well as our revised results of the $1^- \text{–} 0^+$ transition. Figure 1 indicates that the further detection of the $1^- \text{–} 1^+$ transition will give the $0^- \text{–} 0^+$ inversion splitting from which important information mentioned above will be obtained.

During the writing of this paper, we learned that Davies, Hamilton, and Johnson have also studied the infrared spectrum of this species between 510–1150 cm^{-1} and assigned the $1^+ \text{–} 0^-$ band.[31]

II. EXPERIMENTAL DETAILS

The experimental setup to detect the $1^+ \text{–} 0^-$ band is similar to that previously reported[29] (see Fig. 2). H_3O^+ was generated in the gas mixture of H_2O/H_2 or O_2/H_2 under a high voltage ac discharge. The mixing ratios of H_2O/H_2 and O_2/H_2 were optimized at 1:4 and 1:8, respectively, as later discussed in Sec. IV. The total pressure of the gas mixture was about 1.8 Torr measured by a capacitance monometer. During the discharge the gas mixture was pumped through an 80 cm water cooled Pyrex tube of 1.2 cm i.d. Note that for the $1^- \text{–} 0^+$ band at 10 μm we used longer (150 cm) cell with smaller bore (0.9 cm i.d.). The shorter cell with larger bore

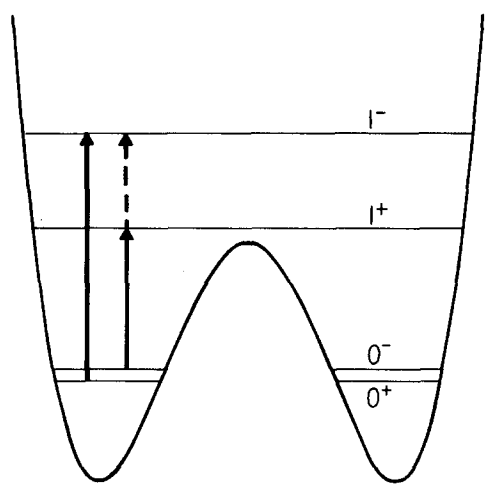

FIG. 1. The double minimum potential for the ν_2 inversion-vibration motion in H_3O^+. The observed $1^- \text{–} 0^+$ and $1^+ \text{–} 0^-$ transitions are shown in the solid lines. The future observation of the $1^- \text{–} 1^+$ transition shown in the dashed line will determine the ground state inversion splitting.

[a] Present address: Dow Chemical Company, Midland, Michigan 48640.

 0021-9606/85/125368-05$02.10

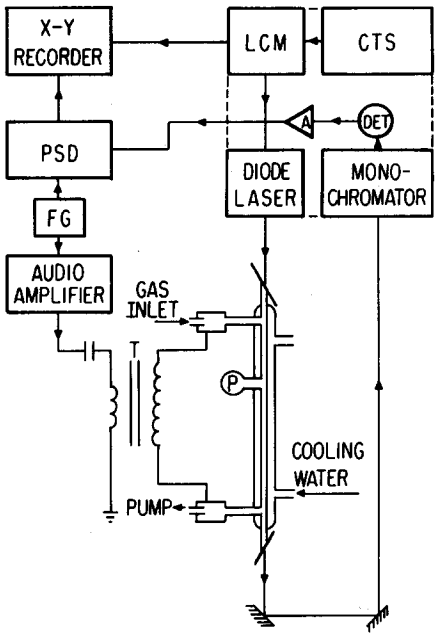

FIG. 2. The experiment layout. LCM and CTS are laser control module and cryogenic temperature stabilizer of LS-3, respectively, FG is a function generator, A is a preamplifier, T is a step-up transformer, and P is a pressure gauge.

was needed for 20 μm because of the more divergent laser beam. The ion density of H_3O^+, estimated from the total power absorption coefficient, was about $\sim 10^{11}$ cm^{-3} (see Sec. III B). The sinusoidal output from a function generator was amplified by an audio amplifier and applied to the discharge electrodes through a step-up transformer to match the high impedence of the discharge. The discharge frequency was kept at 3 kHz with a current of 150 mA rms and voltage of 5 KV, peak to peak. The discharge temperature in the center of the cell was estimated to be about 500 K from the observed relative intensities of the lines.

The infrared radiation source was provided by the LS-3 IR spectrometer. Mesa-stripe geometry diode lasers from Laser Analytics were used to cover the 1^+–0^- band at 20 μm over ~ 180 cm^{-1} (one diode) and the 1^-–0^+ band at 10 μm over ~ 230 cm^{-1} (two diodes). The coverage was not continuous as is usually the case for a diode laser. The infrared radiation, passed through the discharge tube and a monochromator, was detected by HgCdTe detectors; this arrangement minimized the thermal noise of the discharge entering the detector. The absorption signal from the detector was amplified and then processed through a phase sensitive detector and displayed on a X–Y recorder. The FTIR spectra of SO_2 and D_2CO gases kindly provided by Johns of Herzberg Institute of Astrophysics were used as frequency references for the 1^+–0^- and the 1^-–0^+ bands respectively.

III. OBSERVED SPECTRUM

A. Spectrum and analysis

Totally, 34 lines have been measured for the 1^+–0^- band and 33 lines for the 1^-–0^+ band. They are listed in Table I. The obviously missing lines of a series are due to noncontinuous coverage of diode lasers. For the 1^-–0^+ band, additional high J lines in the R branch $R(4)\sim R(7)$ measured by Lemoine and Destombes are also listed. The accuracy of the measurement for the 1^+–0^- band is 0.002

TABLE I. Absorption line positions (in cm^{-1}) of 1^-–0^+ and 1^+–0^- bands.

1^-–0^+ band		1^+–0^- band	
$P(5,0)$	831.709(7)	$P(3,2)$	459.317(0)
$P(4,1)$	858.779(−2)	$P(3,1)$	460.110(−1)
$P(4,3)$	864.008(3)	$Q(12,12)$	510.775(2)
$P(3,1)$	884.365(−2)	$Q(11,11)$	513.092(−1)
$P(3,2)$	886.359(−1)	$Q(13,12)$	513.379(1)
$Q(6,4)$	942.351(4)	$Q(10,10)$	515.270(0)
$Q(5,3)$	944.138(−2)	$Q(13,11)$	518.863(−2)
$Q(8,7)$	947.961(−14)	$Q(8,8)$	519.113(−3)
$Q(7,6)$	947.981(−4)	$Q(6,6)$	522.178(−1)
$Q(9,8)$	948.215(0)	$Q(8,7)$	522.724(1)
$Q(6,5)$	948.239(−3)	$Q(5,5)$	523.384(1)
$Q(10,9)$	948.705(−4)	$Q(4,4)$	524.356(−1)
$Q(5,4)$	948.742(−4)	$Q(6,5)$	524.920(1)
$Q(3,2)$	950.499(−5)	$Q(3,3)$	525.093(0)
$Q(2,1)$	951.764(−1)	$Q(9,7)$	525.169(6)
$Q(13,12)$	951.779(5)	$Q(2,2)$	525.583(0)
$Q(2,2)$	953.806(−1)	$Q(5,4)$	525.649(−1)
$Q(3,3)$	953.897(−2)	$Q(1,1)$	525.833(5)
$Q(1,1)$	953.975(1)	$Q(4,3)$	526.132(−2)
$Q(4,4)$	954.254(3)	$Q(2,1)$	526.347(−1)
$Q(5,5)$	954.867(0)	$Q(3,2)$	526.366(0)
$Q(6,6)$	955.752(2)	$Q(9,6)$	528.806(−5)
$Q(7,7)$	956.921(14)	$Q(5,2)$	528.859(−8)
$Q(8,8)$	958.352(4)	$Q(8,5)$	529.218(6)
$Q(9,9)$	960.083(2)	$Q(6,3)$	529.238(3)
$Q(10,10)$	962.120(2)	$R(0,0)$	548.187(−1)
$Q(11,11)$	964.474(0)	$R(1,1)$	570.549(5)
$Q(12,12)$	967.158(−6)	$R(2,1)$	593.383(−1)
$R(1,0)$	996.064(1)	$R(2,0)$	593.637(0)
$R(2,2)$	1017.951(0)	$R(3,2)$	615.691(−1)
$R(3,0)$	1033.281(−2)	$R(3,1)$	616.454(−4)
$R(3,1)$	1033.963(12)	$R(4,2)$	638.990(1)
$R(3,3)$	1039.391(−2)	$R(4,1)$	639.775(−2)
$R(4,1)^a$	1050.952(−3)	$R(4,0)$	640.045(2)
$R(4,2)^a$	1052.920(−9)		
$R(5,0)^a$	1066.348(8)		
$R(5,1)^a$	1066.978(5)		
$R(5,3)^a$	1072.124(−10)		
$R(6,3)^a$	1087.070(13)		
$R(7,1)^a$	1096.391(−6)		

[a] Lines measured by Lemoine and Destombes (Ref. 30).

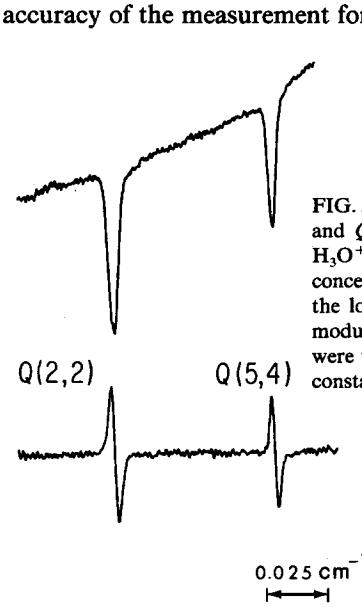

FIG. 3. Two Q branch transitions $Q(2,2)$ and $Q(5,4)$ of ν_2 1^+–0^- transition of H_3O^+. The upper trace shows the $2f$ concentration modulation signals and the lower trace shows the $1f$ velocity modulation signals. Both $1f$ and $2f$ lines were taken in the same scale. The time constant of detection was 1 s.

TABLE II. Molecular constants (in cm^{-1}).

	1^-–0^+ transition		1^+–0^- transition	
	Observed	Predicted[b]	Observed	Predicted[c]
ν_0	954.4003(25)	992	525.8237(13)	543.5
B_1	10.6973(5)	10.66	11.1838(4)	11.24
B_0	11.2537(6)	11.14	11.0558(4)	11.06
$(C_1 - B_1) - (C_0 - B_0)$	0.6863(3)	0.67	− 0.2521(2)	− 0.34
$D_{1,J}$[a]	5.14(10)	7.2	6.47(11)	10.83
$D_{0,J}$	13.02(16)	11.0	10.08(10)	12.41
$D_{1,JK}$	− 6.53(46)	− 10.7	− 6.62(85)	− 16.03
$D_{0,JK}$	− 27.51(54)	− 22.5	− 17.02(85)	− 22.58
$D_{1,K} - D_{0,K}$	− 13.82(9)	− 9.2	− 7.65(4)	− 6.09

[a] Centrifugal distortion constants in unit of 10^{-4} cm^{-1}.
[b] Reference 25.
[c] Reference 27.

cm^{-1}, whereas for the 1^-–0^+ band it was about 0.005 cm^{-1}. Figure 3 shows two Q branch lines of the 1^+–0^- band with typical signal-to-noise ratio and linewidth. Both velocity modulation ($1f$) and concentration modulation ($2f$) signals are shown in the same scale. The best signal-to-noise ratios were 50 for $2f$ detection and 15 for $1f$ detection with the time constant of 1 s. The decrease of the signal strength for the $1f$ detection compared with that for the $2f$ detection is contrary to our previous observations in the 3–4 μm region and 10 μm region where the velocity modulation was more effective. This decrease in the efficiency of modulation at 20 μm suggests that the Doppler broadening is not as dominant in this region as in the others. This fact may be due to the large laser linewidth in this region or to the other broadening effects such as pressure broadening or "transit" broadening. We will discuss the last effect in a separate paper.

Since the separation of the J, K dependence of inversion from that of rotational energy is impossible, the rotational energy level is expressed in terms of the effective rotational constants as[32]

$$W(J,K) = BJ(J+1) + (C - B)K^2 - D_J J^2(J+1)^2 - D_{JK} J(J+1)K^2 - D_K K^4. \quad (1)$$

The observed spectra were fitted by least-square analysis, and the resulting molecular constants and their standard deviations are listed in Table II. The inclusion of higher order (sextic) centrifugal distortion constants did not significantly improve the least-square fitting of our experimental data and hence was dropped. The theoretical prediction of the effective rotational constants by Bunker, Kraemer, and Spirko and those by Bunker, Amano, and Spirko are also listed in Table II for comparison. The standard deviation of lines for the 1^+–0^- transition is 0.003 cm^{-1} which is comparable to our present experimental accuracy of 0.002 cm^{-1}. Two revisions were needed for the results of the 1^-–0^+ band reported earlier by Haese and Oka.[29] First, the assignment of four pairs of very close lines have been interchanged in order to give better least-square fitting and to confirm more closely to theoretical intensity ratios. This correction has already been made by Davies *et al.*[31] Second, we revised some of the data for which lack of accurately measured reference lines caused large errors. After these revisions, the standard deviation of fitting is 0.006 cm^{-1} which is comparable to the experimental accuracy of 0.005 cm^{-1}.

It is interesting to compare the observed band origins with those predicted by theory, as the latter have greatly aided our search efforts. In Table III we list the band origins of both transitions calculated by five different groups as well as our experimental results. It shows good agreement between the theory and the experiment.

B. Absorption intensities

In order to estimate the number density of the H_3O^+ molecular ion in the discharge, and further to test the theoretically predicted relative band intensities of the 1^-–0^+ (10 μ) and the 1^+–0^- (20 μ) transitions,[26] we have measured the fractional infrared absorption $\Delta I/I$ by dividing the voltage of the $2f$ signal by that of the total power. The values of $\Delta I/I$ were determined to be 0.16% and 0.38% for the Q(3,3) lines of the 1^-–0^+ band and the 1^+–0^- bands, respectively. Dividing these values by the discharge cell lengths employed (150 and 80 cm), we obtain the absorption coefficient α of

TABLE III. Comparison of experimental observed band origin ν_0 with theoretical predictions (in cm^{-1}).

	This work	BKS[a]	BAS[b]	STO[c]	BRR[d]	DKR[e]	NSK[f]
1^+–0^- transition	525.824	511	543.5	560	559	513	539.417
1^-–0^+ transition	954.400	992	954.4	985	961	1037	1075.217

[a] Reference 25.
[b] Reference 27. Prediction of 1^+–0^- band origin based on the adjustment from observed 1^-–0^+ band origin.
[c] Reference 28.
[d] Reference 26.
[e] Reference 22.
[f] Reference 24.

1.1×10^{-5} and 4.8×10^{-5} cm^{-1}, respectively. The ratio of these values is 0.23; which agrees well with the purely theoretical prediction of 0.27 by Botchwina *et al.*[26] (assuming a temperature of 500 K and equal ion densities). This agreement suggest a reliability of the theoretical prediction for the ratios of absorption intensity of 1^-–0^+ or 1^+–0^- band with 1^-–1^+ band which is important for further experiments.

The transition dipole moments μ_{if} calculated by Botchwina *et al.*[26] were 0.302 and 0.673 D for the 1^-–0^+ and the 1^+–0^- transitions, respectively. The absorption cross sections σ are calculated from the following equation[17]:

$$\sigma=\frac{\pi^2}{3}\left(\frac{2mhB^2C}{k^4T_{\rm trans}T_{\rm rot}^3}\right)^{1/2}\mu_{if}^2\cdot S(I,K)(2J+1)\times\exp\left[-\frac{h\nu_i}{kT_{\rm vib}}-\frac{h\,[BJ(J+1)+(C-B)K^2]}{kT_{\rm rot}}\right]\times\left[1-\exp\left(-\frac{h\nu_{if}}{kT_{\rm vib}}\right)\right]/Q_{\rm vib}, \quad (2)$$

where B and C are rotational constants of H_3O^+, $h\nu_i$ is the inversion-vibration energy of the lower state, $h\nu_{if}$ is the energy difference of the transition, $Q_{\rm vib}$ is the vibrational partition function, $S(I,K)$ is the nuclear spin statistical weight, and m is the mass of H_3O^+. $T_{\rm trans}$, $T_{\rm rot}$, and $T_{\rm vib}$ are the translational, rotational, and vibrational temperature of H_3O^+ in dicharge, respectively. In deriving Eq. (2) a Doppler broadening Gaussian line shape is assumed. We thus have the cross sections of 8.5×10^{-17} and 3.1×10^{-16} cm^2 for the $Q(3,3)$ transitions of the 1^-–0^+ and the 1^+–0^- bands, respectively, if we assume the equal translational, rotational, and vibrational temperature of 500 K. The actual vibrational temperature may be higher leading to the smaller values of cross section.

From the observed absorption coefficient α and the cross section σ calculated above, we estimated the H_3O^+ ion densities of 1.3×10^{11} and 1.5×10^{11} cm^{-3} for the two cases from $n=\alpha/\sigma$. Because of the uncertainties both in observed α and in calculated σ, these values have rather high uncertainties but will give right order of magnitude.

Actual ion density during the discharge may be higher because of the duty cycle of the dicharge current which was observed to be about 1/2 on a monitoring oscilloscope. The value of averaged ion concentration 1.4×10^{11} cm^{-3} agrees approximately with the electron density n_e (1.2×10^{11} cm^{-3}) in the discharge calculated from

$$n_e=I/eV_eS, \quad (3)$$

using the experimental current density $I/S=130$ mA/cm^2 rms and the electron migration velocity $V_e=7\times10^6$ cm/s.[33]

IV. FORMATION OF H_3O^+ IN THE DISCHARGE

In order to understand reaction processes in the discharge leading to the formation of H_3O^+, we have measured the variation of H_3O^+ line intensities as a function of the mixing ratio in the O_2/H_2 and H_2O/H_2 discharges. The observed results are shown in Fig. 4. The optimum conditions were reached when the mixing ratios were 1:8 and 1:4, respectively. The O_2/H_2 mixture gave slightly stronger H_3O^+ signal than the H_2O/H_2 mixture. The clear difference between the two mixtures was the sharp decrease of the signal in the O_2/H_2 discharge, compared with the gradual decrease in the H_2O/H_2 discharge with increases of O_2 or H_2O.

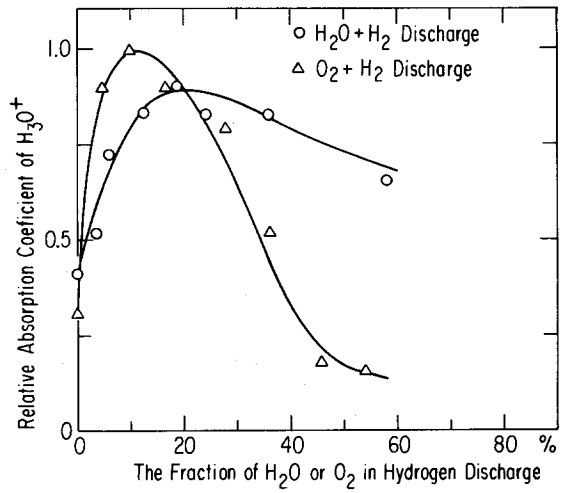

FIG. 4. The relative absorption coefficient of H_3O^+ vs the fraction of H_2O or O_2 in hydrogen glow discharge. The peak value of the absorption coefficient of H_3O^+ in O_2/H_2 discharge is set as unity.

In the H_2O/H_2 discharge, the formation of H_3O^+ must start from the ionization of H_2 and H_2O. The electronic temperature in the discharge can be roughly estimated to be 2.3 eV[33] from the discharge conditions. Thus the ionization is achieved by high energy electrons in the tail of the Boltzmann distribution. Our calculation based on the known ionization cross sections[34] shows that the ionization of H_2 and H_2O occurs with similar rates in spite of the higher ionization potential in H_2 (15.4 eV) than in H_2O (12.6 eV). The H_2^+ and H_2O^+ ions thus produced proceed to form H_3O^+ by the following reactions[3,35]:

$$H_2O^+ \xrightarrow[-H]{H_2} H_3O^+, \quad (4)$$

$$H_2^+ \xrightarrow[-H]{H_2} H_3^+ \xrightarrow[-H_2]{H_2O} H_3O^+. \quad (5)$$

Excessive water does not hinder the series of reactions other than producing H_3O^+ directly through the reaction with H_2^+ or possibly lowering the electron temperature and thus reducing the efficiency of ionization.

In the O_2/H_2 discharge, the first steps of reactions are the electron ionization to produce H_2^+ and O_2^+, the impact dissociation to produce O and O^-, and the dissociative ionization to produce O^+.[34,36] Although the rate of the dissociative ionization is calculated to be two orders of magnitude lower than those of ionization and impact dissociation,[37] the atomic O^+ ion can directly lead to H_3O^+ through the series of ion–molecule reactions[35]

$$O^+ \xrightarrow[-H]{H_2} OH^+ \xrightarrow[-H]{H_2} H_2O^+ \xrightarrow[H]{H_2} H_3O^+, \quad (6)$$

which occurs very quickly because of the abundant H_2. Other products, H_2^+, O_2^+, and O have to go through at least one more slow process before the formation of H_3O^+. It is

known that much O_2^+ is produced in the metastable $^4\pi_u$ state[37,38] which is 4.1 eV above the ground state. Such O_2^+ can form OH^+ efficiently though exothermic reaction

$$O_2^+(^4\pi) + H_2 \rightarrow OH^+ + OH. \quad (7)$$

This reaction is endothermic for the ground state O_2^+ and requires large relative energy.[39] An excessive amount of oxygen will hinder the formation of H_3O^+ by charge transfer reaction with OH^+ and H_2O^+, thus shifting the plasma ion concentration from H_3O^+ to O_2^+. The O_2^+ ion is known to be quite abundant in such discharges; even in pure H_2O discharges at those pressures O_2^+ can dominate H_3O^+ as is observed in direct mass spectra.[40]

It was suggested by the referee to this paper that while ions are initially produced by the reactions given above, the H_2O molecule which always exist abundantly in discharges containing O_2 and H_2 may lead to H_3O^+ through the reactions considered above for the H_2O/H_2 mixture. We have measured the intensities of rotational absorption lines of H_2O and estimated the abundance of H_2O to be about 1% of O_2. Such H_2O also produces H_3O^+ through reactions (4) and (5).

V. SUMMARY

The new feature of this work is the observation of the 1^+–0^- band of H_3O^+ and the determination of molecular constants for the levels involved. The absorption intensities have been studied and compared with the theoretical prediction. The chemical formation scheme for the H_3O^+ has been discussed.

Our futher work will focus on the 1^-–1^+ transition in Fig. 1 from which to determine the inversion splitting of the ground state. Experimental work has been carried out for this transition and we have found several lines around 380 cm^{-1} region. We have measured 17 lines for the 1^-–0^+ band of $H^{18}O^+$ isotopic species, the detail of which will be published separately.

Note added in proof: Recently[41] we have observed the $1^- \leftarrow 1^+$ band of H_3O^+ and determined the ground state inversion splitting to be 55.3462 ± 0.0055 cm^{-1}.

ACKNOWLEDGMENTS

We wish to thank J. W. Johns for sending us the high quality FTIR spectra of D_2CO and SO_2 which were used for frequency calibration. We are also grateful to P. Botschwina, P. R. Bunker, and K. Ohno for sending us their theoretical papers prior to publication. We acknowledge discussion with J. Berkowitz on the chemistry of O_2^+ ($^4\pi_u$). This work was supported by NSF grant No. 8113097. We also acknowledge the partial support by the Camille and Henry Dreyfus Foundation.

[1] R. P. Bell, *The Proton in Chemistry* (Cornell University, Ithaca, 1973).
[2] M. Eigen, Angew. Chem. Int. Ed. **3**, 1 (1964).
[3] E. Herbst and Klemperer, Astrophys. J. **185**, 505 (1973).
[4] T. de Jong, A. Dalgarno, and W. Boland, Astron. Asrophys. **91**, 68 (1980).
[5] S. S. Prasad and W. T. Huntress, Jr., Astrophys. J. Suppl. **43**, 1 (1980).
[6] D. E. Bethell and N. Sheppard, J. Chem. Phys. **21**, 1421 (1953).
[7] C. C. Ferriso and D. F. Hornig, J. Am. Chem. Soc. **75**, 4113 (1953).
[8] Th. Ackermann, Z. Phys. Chem. **27**, 253 (1961).
[9] J. T. Mullhaupt and D. F. Hornig, J. Chem. Phys. **24**, 169 (1956).
[10] R. E. Richards and J. A. S. Smith, Trans. Faraday Soc. **47**, 1261 (1951).
[11] J. A. S. Smith, Q. Rev. Chem. Soc. London **7**, 279 (1953).
[12] Y. Kakiuchi, H. Shono, H. Komatsu, and K. Kigoshi, J. Chem. Phys. **19**, 1069 (1951).
[13] P. A. Giguére and S. Turrell, Can. J. Chem. **54**, 3477 (1976).
[14] P. A. Giguére and C. Madec, Chem. Phys. Lett. **37**, 569 (1976).
[15] H. A. Schwarz, J. Chem. Phys. **67**, 5525 (1977).
[16] M. H. Begemann, C. S. Gudeman, J. Pfaff, and R. J. Saykally, Phys. Rev. Lett. **51**, 554 (1983); M. H. Begemann and R. J. Saykally, J. Chem. Phys. (in press).
[17] C. H. Townes and A. L. Schawlow, *Microwave Spectroscopy* (Dover, New York, 1975).
[18] W. Gordy and R. L. Cook, *Microwave Molecular Spectra* (Interscience, New York, 1970).
[19] H. Lischka, Theor. Chim. Acta (Berlin) **31**, 39 (1973).
[20] P. A. Kollman and C. F. Bender, Chem. Phys. Lett. **21**, 271 (1973).
[21] H. Lischka and V. Dyczmons, Chem. Phys. Lett. **23**, 167 (1973).
[22] G. H. F. Diercksen, W. P. Kraemer, and B. O. Roos, Theor. Chim. Acta (Berlin) **36**, 249 (1975).
[23] V. Špirko and P. R. Bunker, J. Mol. Spectrosc. **95**, 226 (1982).
[24] S. E. Novick, R. M. Stevens, and W. Klemperer (privat communication).
[25] P. R. Bunker, W. P. Kraemer, and V. Špirko, J. Mol. Spectrosc. **101**, 180 (1983).
[26] P. Botschwina, P. Rosmus, and E.-A. Reinsch, Chem. Phys. Lett. **102**, 299 (1983).
[27] P. R. Bunker, T. Amano, and V. Spirko, J. Mol. Spectrosc. **107**, 208 (1984).
[28] N. Shida, K. Tanaka, and K. Ohno, Chem. Phys. Lett. **104**, 575 (1984).
[29] N. N. Haese and T. Oka, J. Chem. Phys. **80**, 572 (1984).
[30] B. Lemoine and J. L. Destombes, Chem. Phys. Lett. **111**, 284 (1984).
[31] P. B. Davies, P. A. Hamilton, and S. A. Johnson, J. Opt. Soc. Am **B2**, 1985 (in press).
[32] G. Herzberg, *Molecular Structure and Molecular Spectra* (Van Nostrand Reinhold, New York, 1945), Vol. II.
[33] A. von Engel, *Ionized Gases*, 2nd ed. (Clarendon, Oxford, 1965).
[34] L. J. Kieffer, At. Data **1**, 19 (1969).
[35] W. T. Huntres Jr., Astrophys. J. Suppl. Ser. **33**, 495 (1977).
[36] G. J. Schulz, NSRDS NBS **50**, 47 (1973).
[37] M. Tadjeddine, R. Aboual, P. C. Crosby, B. A. Huber, and J. T. Moseley, J. Chem. Phys. **69**, 718 (1978).
[38] A. Carrington, P. G. Roberts, and P. J. Sarre, Mol. Phys. **35**, 512 (1978).
[39] M. M. Chiang, E. A. Gislason, B. H. Mahan, C. W. Tsao, and A. S. Werner, J. Phys. Chem. **75**, 1426 (1971).
[40] N. N. Haese, Thesis, 1981.
[41] Di-Jia Liu and T. Oka, Phys. Rev. Lett. **54**, 1787 (1985).